

Synchronization and firing mode transition of two neurons in a bilateral auditory system driven by a high--low frequency signal

Charles Omotomide Apata, Yi-Rui Tang(唐浥瑞), Yi-Fan Zhou(周祎凡), Long Jiang(蒋龙), and Qi-Ming Pei(裴启明)

Citation: Chin. Phys. B, 2024, 33 (**5**): 058704. DOI: 10.1088/1674-1056/ad1a8e

What follows is a list of articles you may be interested in

Dynamical behaviors in discrete memristor-coupled small-world neuronal networks

Jieyu Lu(鲁婕妤), Xiaohua Xie(谢小华), Yaping Lu(卢亚平), Yalian Wu(吴亚联), Chunlai Li(李春来), and Minglin Ma(马铭磷)

Chin. Phys. B, 2024, 33 (**4**): 048701. DOI: 10.1088/1674-1056/ad1483

Dynamical behavior of memristor-coupled heterogeneous discrete neural networks with synaptic crosstalk

Minglin Ma(马铭磷), Kangling Xiong(熊康灵), Zhijun Li(李志军), and Shaobo He(贺少波)

Chin. Phys. B, 2024, 33 (**2**): 028706. DOI: 10.1088/1674-1056/aceee9

Paradoxical roles of inhibitory autapse and excitatory synapse in formation of counterintuitive anticipated synchronization

Xue-Li Ding(丁学利), Hua-Guang Gu(古华光), Yu-Ye Li(李玉叶), and Yan-Bing Jia(贾雁兵)

Chin. Phys. B, 2023, 32 (**8**): 088701. DOI: 10.1088/1674-1056/acc450

Synchronization coexistence in a Rulkov neural network based on locally active discrete memristor

Ming-Lin Ma(马铭磷), Xiao-Hua Xie(谢小华), Yang Yang(杨阳), Zhi-Jun Li(李志军), and Yi-Chuang Sun(孙义闯)

Chin. Phys. B, 2023, 32 (**5**): 058701. DOI: 10.1088/1674-1056/acb9f7

Hopf bifurcation and phase synchronization in memristor-coupled Hindmarsh-Rose and FitzHugh-Nagumo neurons with two time delays

Zhan-Hong Guo(郭展宏), Zhi-Jun Li(李志军), Meng-Jiao Wang(王梦蛟), and Ming-Lin Ma(马铭磷)

Chin. Phys. B, 2023, 32 (**3**): 038701. DOI: 10.1088/1674-1056/aca601

Synchronization and firing mode transition of two neurons in a bilateral auditory system driven by a high–low frequency signal

Charles Omotomide Apata, Yi-Rui Tang(唐浥瑞), Yi-Fan Zhou(周祎凡), Long Jiang(蒋龙)[†], and Qi-Ming Pei(裴启明)[‡]

School of Physics and Optoelectronic Engineering, Yangtze University, Jingzhou 434023, *China*

(Received 21 October 2023; revised manuscript received 14 December 2023; accepted manuscript online 4 January 2024)

The FitzHugh–Nagumo neuron circuit integrates a piezoelectric ceramic to form a piezoelectric sensing neuron, which can capture external sound signals and simulate the auditory neuron system. Two piezoelectric sensing neurons are coupled by a parallel circuit consisting of a Josephson junction and a linear resistor, and a binaural auditory system is established. Considering the non-singleness of external sound sources, the high–low frequency signal is used as the input signal to study the firing mode transition and synchronization of this system. It is found that the angular frequency of the high–low frequency signal is a key factor in determining whether the dynamic behaviors of two coupled neurons are synchronous. When they are in synchronization at a specific angular frequency, the changes in physical parameters of the input signal and the coupling strength between them will not destroy their synchronization. In addition, the firing mode of two coupled auditory neurons in synchronization is affected by the characteristic parameters of the high–low frequency signal rather than the coupling strength. The asynchronous dynamic behavior and variations in firing modes will harm the auditory system. These findings could help determine the causes of hearing loss and devise functional assistive devices for patients.

Keywords: piezoelectric ceramic, Josephson junction, auditory neuron, synchronization

PACS: 87.19.lm, 87.15.A–, 87.19.ll **DOI:** 10.1088/1674-1056/ad1a8e

1. Introduction

The mammalian ear has a unique, curly, three-dimensional structure that is particularly suitable for extracting specific components of mechanical stimulation reaching the ear.[1] These mechanical stimuli propagate in a particular direction until they pass through hair cells, which convert the information on the specific frequency band and propagation direction of mechanical stimuli into electrical signals. The mammalian cochlea can screen the spectral characteristics of signals. The signals are transmitted to the brain through auditory neurons, and finally the organism perceives sound.

In artificial intelligence and neuroscience, embedding piezoelectric ceramic into neural circuits can simulate the functioning of human ears, thereby enabling the signal transmission process to the brain to be studied. Piezoelectric ceramic is an intelligent material that converts mechanical effects (such as pressure, motion or vibration) into electrical signals, and vice versa.[2–4] The generated electrical signal drives the neural circuit to produce various firing modes and wake the nerve center. It can be proved that simple neural circuits embedded with piezoelectric ceramic can be used to repair hearing damage.[2]

Although different animals can only hear sound waves of specific frequencies, signals from authentic sources rarely exhibit a single frequency. In addition, neurons can synchronously receive multiple signal inputs through various channels. Therefore, a high–low frequency (HLF) signal has been widely used in the nervous system. These two frequency signals correspond to different signal input channels in neurons, so the bursting neurons driven by the HLF signal display two distinct time scales.[5] It was found that high-frequency stimulation can increase the absorption of drugs by brain cells and enhance the biodegradation of microorganisms through resonance. Ultrasonic irradiation with different frequencies can improve cavitation yield.[6] The electrical activity mode of the FitzHugh–Nagumo (FHN) neuron driven by HLF electromagnetic radiation can undergo continuous transitions of static, peak, burst and mixed states by changing the amplitude and angular frequency of the HLF signal.[7] When a mixed signal composed of a low frequency and a high frequency is synchronously applied to Hindmarsh–Rose (H–R) neurons, the response of electrical activity depends mainly on amplitude rather than frequency.[8] In addition, whether the electric field is considered or not, multiple vibration resonances can be observed in a single H–R neuron model driven by an external stimulation current composed of HLF signals.[9]

For most mammals, especially humans, the two ears can effectively receive and synchronously encode external sound signals, thereby synchronizing the activities of two auditory neurons. In an auditory system without synaptic coupling, two identical piezoelectric sensing neurons can achieve synchronous pulses, spikes and periodic discharges under the

[†]Corresponding author. E-mail: jianglong@yangtzeu.edu.cn
[‡]Corresponding author. E-mail: qmpei@yangtzeu.edu.cn

© 2024 Chinese Physical Society and IOP Publishing Ltd

same periodic stimulation.[2]

From a medical standpoint, it may be asserted that the two ears of an individual are indirectly interconnected. In artificial intelligence and neuroscience, which electronic components can be used to realize this connection of two middle ears? It has been found that embedding various electronic components in neural circuits enables detection and encoding of external optical signals, electromagnetic fields, thermal signals, etc.[2–4] A memristor can represent the relationship between magnetic flux and charge.[10–12] When a memristor is connected to a neural circuit, the impact of electromagnetic induction on neurons can be estimated.[5,13–16] Because the resistance value of a thermistor varies with temperature,[17–20] neural circuits with thermistors can be used as biophysical thermosensitive neurons.[21–24] Phototubes can convert optical signals into electrical signals. So neural circuits coupled with phototubes can be used as biophysical light-dependent neurons,[25–28] which have potential application value in the design of artificial eyes. Since the channel current through a Josephson junction depends on the external magnetic field,[29,30] the neuron circuit embedded in the Josephson junction can be used to sense the influence of the magnetic field.[31–34]

Among the aforementioned electronic components, the Josephson junction is a promising choice for realizing indirect connection of two middle ears. The human brain contains approximately 86 billion neurons, but only consumes about 15 W of energy during regular operation,[35] indicating a very low energy consumption. On the other hand, in signal transmission between neurons, electrical signals will be transmitted between neurons in the form of pulses and then gradually fade away. When a specific action is repeated, the neuron can be called up at any time, reaching its peak and forming fluctuating pulses, with faster speed and lower energy consumption. A Josephson junction can imitate this pulse signal transmission mode of the brain, and also has a low energy consumption.[21]

Therefore, interesting questions are suggested. Can two auditory neurons coupled by a Josephson junction achieve synchronization? If two coupled auditory neurons can achieve synchronization, which factors will affect their firing modes? Does coupling strength have an impact on their synchronization and firing modes? To address these issues, the FHN neuron model embedded in a piezoelectric ceramic was chosen as an auditory neuron. Two auditory neurons were connected through a parallel circuit composed of a Josephson junction and a linear resistor to construct a binaural auditory neuron system. Using the HLF signal as an external sound signal, the synchronization characteristics of this system were studied based on the error function.[2]

This paper is organized as follows. In Section 2, a binaural auditory neuron system is constructed and its circuit equation is derived. Based on the numerical simulation results, the synchronization characters and the firing mode transition of this system are studied in Section 3. We end with conclusions and discussions in Section 4.

2. Auditory neuron circuits and equations

2.1. Mono-ear auditory neuron circuit and equation

Alan Lloyd Hodgkin and Andrew Fielding Huxley performed a voltage clamp experiment on abalone giant axons in 1952 to evaluate the link between membrane current and membrane voltage. They pioneered the Hodgkin–Huxley (H–H) model.[36] This is a nonlinear differential equation set that successfully explains the generation and propagation of action potentials. However, the H–H model is highly nonlinear and complex to grasp intuitively. Richard FitzHugh simplified the H–H model to a second-order nonlinear model in 1961.[37] Nagumo *et al.* designed the corresponding equivalent circuit and simulated it in 1962.[38] This second-order nonlinear model was found to preserve several qualitative traits of the H–H model, such as analytical and numerical properties.[39] This simplified nonlinear model is named the FHN model. Although the equation of the FHN model is simple, it can reflect the main characteristics of neuronal discharge activity so is widely used to study the firing activity of primary neurons. If appropriate parameters are selected, the FHN model can replicate the basic input and output characteristics of real neurons, such as the phase-locked, chaotic response of semi-periodic excitation.

The corresponding equivalent circuit diagram of the FHN model is shown in Fig. 1(a). V_S is a time-varying voltage source and E is another constant voltage source. C, L and NR refer to capacitor, induction coil and nonlinear resistor, respectively. R_S and R are both linear resistors.

Due to the ability of piezoelectric ceramics to convert mechanical effects into electrical signals, a mono-ear auditory neuron circuit can be obtained by replacing the time-varying voltage source V_S in the FHN neuron circuit with a piezoelectric ceramic PC, as shown in Fig. 1(b).

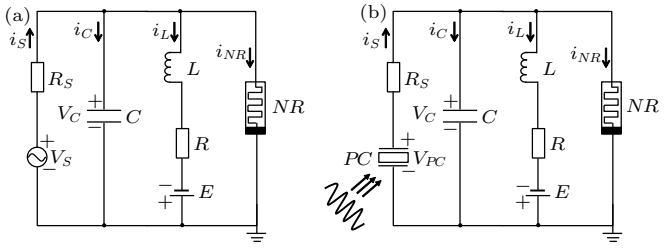


Fig. 1. Schematic diagram of a FHN neuron circuit driven by different power sources.[2,3] E is a constant voltage source. C, L and NR represent capacitor, induction coil and nonlinear resistor, respectively. R_S and R are linear resistors. (a) Driven by a time-varying voltage source V_S. (b) Driven by a piezoelectric ceramic PC.

According to Kirchhoff's law, the circuit equations corresponding to Fig. 1(b) are

$$\begin{aligned} C\frac{\mathrm{d}V}{\mathrm{d}t} &= \frac{V_{PC}-V}{R_S} - i_L - i_{NR}, \\ L\frac{\mathrm{d}i_L}{\mathrm{d}t} &= V + E - Ri_L. \end{aligned} \tag{1}$$

These are two nonlinear ordinary differential equations. The first equation describes the rapid evolution of neuron membrane voltage, in which the variable V represents the output voltage of the capacitor, i.e., the membrane potential. The second equation describes the slow 'recovery' effect of sodium channel and potassium channel deactivation, in which i_L represents the induced current generated on the induction coil. The variable V_{PC} represents the voltage generated by the external force acting on the piezoelectric ceramic, which is determined by the material constant, the thickness of the piezoelectric ceramic and the pressure due to the external force acting on it.

The variable i_{NR} represents the conduction current flowing through the nonlinear resistor. It is usually taken as

$$i_{NR} = -\frac{1}{\rho}\left(V - \frac{1}{3}\frac{V^3}{V_0^2}\right), \tag{2}$$

where ρ is the normalized resistance and V and V_0 represent the terminal voltage and cut-off voltage flowing through the nonlinear resistor, respectively.[38]

To achieve reliable synchronization control in neurons or neural networks, it is necessary to scale the physical variables and parameters in the circuit equations. The scaling transformation method commonly used in acoustic neuron circuits[2,3] is applied here, namely,

$$\begin{aligned} &x = V/V_0, \quad y = \rho i_L/V_0, \quad \tau = t/(\rho C), \quad \lambda = \rho/R_S, \\ &u_{PC} = V_{PC}/V_0, \quad a = E/V_0, \quad b = R/\rho, \quad c = \rho^2 C/L. \end{aligned} \tag{3}$$

Then, an expression equivalent to Eq. (1) can be obtained as

$$\begin{aligned} \frac{\mathrm{d}x}{\mathrm{d}\tau} &= x(1-\lambda) - \frac{1}{3}x^3 - y + \lambda u_{PC}, \\ \frac{\mathrm{d}y}{\mathrm{d}\tau} &= c(x + a - by). \end{aligned} \tag{4}$$

In Eq. (4), a, b, c and λ are determined by the physical properties of the electronic components contained in the circuit, and can be called system parameters. u_{PC} is determined by the external driving signal of the neural circuit. Different external signals can trigger different kinds of voltage source signals. For simplicity, the periodic HLF[7,15,40] signal is considered here

$$\lambda u_{PC} = A\cos(\omega\tau) + B\cos(N\omega\tau), \tag{5}$$

in which A is the amplitude of low-frequency signal, B is the amplitude of the high-frequency signal, ω is the angular frequency and N is the frequency ratio of the high-frequency signal to the low-frequency signal. To highlight the presence of the high-frequency signal, only frequency ratios N greater than 5 are considered in this paper, namely, $N \geq 5$.

2.2. Binaural auditory neuron circuit and equation

To construct a binaural auditory neuron system, two auditory neurons can be connected using specific electronic components. The parallel circuit composed of a Josephson junction and a linear resistor R_j is used as the coupling channel. On the one hand, the Josephson junction can not only simulate the pulse signal transmission mode of the brain but also has a very low energy consumption. On the other hand, the linear resistor R_j can carry some current to protect the Josephson junction. The circuit diagram is shown in Fig. 2. I_C represents the maximal node current through the Josephson junction, and φ represents the phase error of the Josephson junction. When the potential difference between the two ends of the Josephson junction is U, the relationship between the phase error φ and the potential difference U satisfies

$$\frac{\mathrm{d}\varphi}{\mathrm{d}t} = \frac{2e}{\hbar}U. \tag{6}$$

Here, the parameters $\hbar$ and e denotes the Planck constant and charge of the electron, respectively.

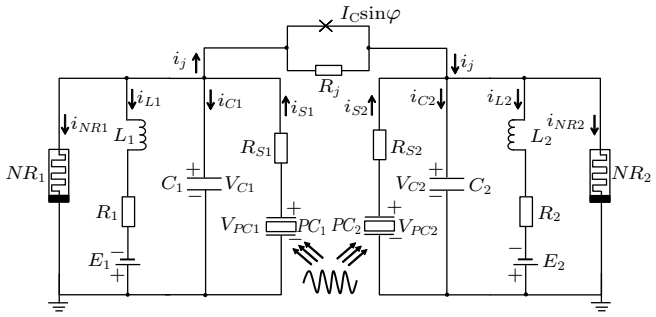


Fig. 2. Schematic diagram of the binaural auditory neuron circuit. Two auditory neurons are coupled by a parallel circuit composed of a Josephson junction and a linear resistor R_j. Variable I_C represents the maximal node current through the Josephson junction, and variable φ represents the phase error of the Josephson junction.

Based on Kirchhoff's law, the circuit equations corresponding to Fig. 2 are obtained as follows:

$$\begin{aligned} C_1\frac{\mathrm{d}V_1}{\mathrm{d}t} &= \frac{V_{PC1}-V_1}{R_{S1}} - i_{L1} + \frac{1}{\rho_1}\left(V_1 - \frac{1}{3}\frac{V_1^3}{V_0^2}\right) \\ &\quad - I_C\sin\varphi - \frac{V_1 - V_2}{R_j}, \\ L_1\frac{\mathrm{d}i_{L1}}{\mathrm{d}t} &= V_1 - R_1 i_{L1} + E_1, \\ C_2\frac{\mathrm{d}V_2}{\mathrm{d}t} &= \frac{V_{PC2}-V_2}{R_{S2}} - i_{L2} + \frac{1}{\rho_2}\left(V_2 - \frac{1}{3}\frac{V_2^3}{V_0^2}\right) \\ &\quad + I_C\sin\varphi + \frac{V_1 - V_2}{R_j}, \\ L_2\frac{\mathrm{d}i_{L2}}{\mathrm{d}t} &= V_2 - R_2 i_{L2} + E_2, \end{aligned}$$

$$\frac{\hbar}{2e}\frac{\mathrm{d}\varphi}{\mathrm{d}t} = V_1 - V_2. \tag{7}$$

To simplify the calculations, two coupled auditory neurons use electronic devices with the same parameters, piezoelectric ceramics with the same quality and nonlinear resistors with the same characteristics, namely, $C_1 = C_2 = C$, $L_1 = L_2 = L$, $E_1 = E_2 = E$, $R_1 = R_2 = R$, $R_{S1} = R_{S2} = R_S$, $V_{PC1} = V_{PC2} = V_{PC}$, $\rho_1 = \rho_2 = \rho$, $V_{01} = V_{02} = V_0$. A scale transformation similar to Eq. (3) is applied to the variables and parameters in Eq. (7) to obtain equivalent circuit expressions

$$\begin{aligned}
\frac{\mathrm{d}x_1}{\mathrm{d}\tau} &= \lambda u_{PC} + x_1(1-\lambda) - \frac{1}{3}x_1^3 - y_1 - \alpha\sin z - \beta(x_1 - x_2),\\
\frac{\mathrm{d}y_1}{\mathrm{d}\tau} &= c(x_1 + a - by_1),\\
\frac{\mathrm{d}x_2}{\mathrm{d}\tau} &= \lambda u_{PC} + x_2(1-\lambda) - \frac{1}{3}x_2^3 - y_2 + \alpha\sin z + \beta(x_1 - x_2),\\
\frac{\mathrm{d}y_2}{\mathrm{d}\tau} &= c(x_2 + a - by_2),\\
\frac{\mathrm{d}z}{\mathrm{d}\tau} &= \gamma(x_1 - x_2).
\end{aligned} \tag{8}$$

Here, the variable $z = \varphi$, the system parameters $\alpha = \rho I_C/V_0$, $\beta = \rho/R_j$ and the coupling strength $\gamma = 2e\rho CV_0/\hbar$. All variables and parameters in Eq. (8) are dimensionless through scale transformation.

To detect the synchronization state of two coupled auditory neurons, an error function[2,3] is introduced

$$\theta(e_x, e_y) = \sqrt{e_x^2 + e_y^2} = \sqrt{(x_1 - x_2)^2 + (y_1 - y_2)^2}. \tag{9}$$

When the error function drops to zero within a certain instantaneous period, dynamic behaviors of two coupled auditory neurons will approach complete synchronization.

3. Simulations and results

In this section, numerical simulation will be carried out for Eq. (8) with different parameters. The synchronization characteristics of the binaural auditory neuron system are studied based on Eq. (9). The algorithm used here is the fourth-order Runge–Kutta method with a time step of 0.01 and a transient period of approximately 100 time units. Two coupled auditory neurons are driven by the same HLF sound signal, as shown in Eq. (5). This paper mainly discusses the effect of the HLF sound signal and coupling strength on the auditory system, so the parameters reflecting the physical characteristics of electronic components in neuron circuits, such as a, b, c, α, β and λ, remain unchanged. For a HLF sound signal, the amplitude of the high-frequency signal can be fixed, and only that of the low-frequency signal is altered to consider the influence of relative amplitude change on this system. Therefore, in the following discussion, let $a = 0.7$, $b = 0.8$, $c = 0.1$, $\alpha = 5$, $\beta = 0.01$, $\lambda = 0.15$ and $B = 0.6$.[38] Considering the correlation between the parameters, the method of controlling two variables, that is, controlling any two of the four variables (N, ω, A, γ), is applied. In order to ensure the effectiveness of the circuit, we take $N \geq 5$, $\omega > 0$, $A > 0$ and $\gamma > 0$. In addition, the initial value is $(x_{10}, x_{20}, y_{10}, y_{20}, z_0) = (0.2, 0.02, 0.1, 0.01, 0.1)$.

3.1. Effects of angular frequency and signal frequency ratio

When $A = 1.0$ and $\gamma = 0.1$, the contour map of error function (θ) with angular frequency (ω) and signal frequency ratio (N) is shown in Fig. 3. Obviously, when $\omega \in (1.35, 2.42)$ and $\omega = 1.06$, $N \in [5, 35]$, the value of the error function $\theta > 0$, indicates that the dynamic behaviors of two coupled auditory neurons are not synchronous. In the remaining region, namely, $\omega \in (0.0, 1.06) \cup (1.06, 1.35] \cup [2.42, 3.0]$ and $N \in [5, 35]$, the value of error function $\theta = 0$, indicating that their dynamic behaviors are synchronous.

Based on Fig. 3, considering $N = 20$, the evolution of membrane potential x_i ($i = 1, 2$, similarly hereinafter) and the corresponding error function θ with sampling time under different angular frequencies ω, such as $\omega = 0.005$, 0.15, 0.5, 1.0, 1.5, 3.0, are shown in Fig. 4. From Figs. 4(b1)–4(b6) it can be seen that when $\omega = 1.5 \in (1.35, 2.42)$ the behaviors of two coupled auditory neurons are asynchronous. For other ω, satisfying $\omega \in (0.0, 1.06] \cup (2.42, 3.0]$, the behaviors of two coupled auditory neurons are synchronous. The above results are consistent with those in Fig. 3. From Figs. 4(a1)–4(a6) it can be seen that with the increasing value of ω, neurons exhibit various firing states: a bursting firing state when $\omega = 0.005$, a spiking firing state when $\omega = 0.15$, a periodical firing state when $\omega = 0.5$, a chaotic firing state when $\omega = 1.0$ and $\omega = 1.5$ and a periodical firing state when $\omega = 3.0$. Therefore, the angular frequency ω also has a significant impact on the firing mode of two coupled auditory neurons.

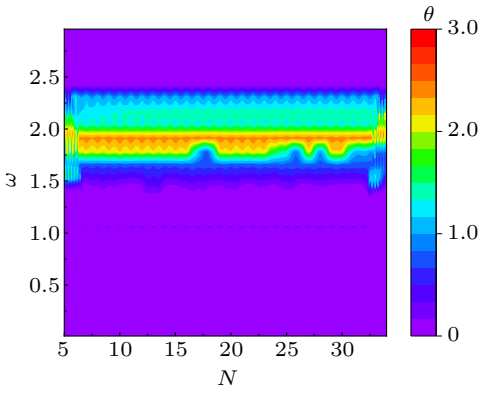


Fig. 3. Contour map of the error function (θ) with angular frequency (ω) and signal frequency ratio (N) when $A = 1.0$ and $\gamma = 0.1$. Other parameter values and initial values are given in the text.

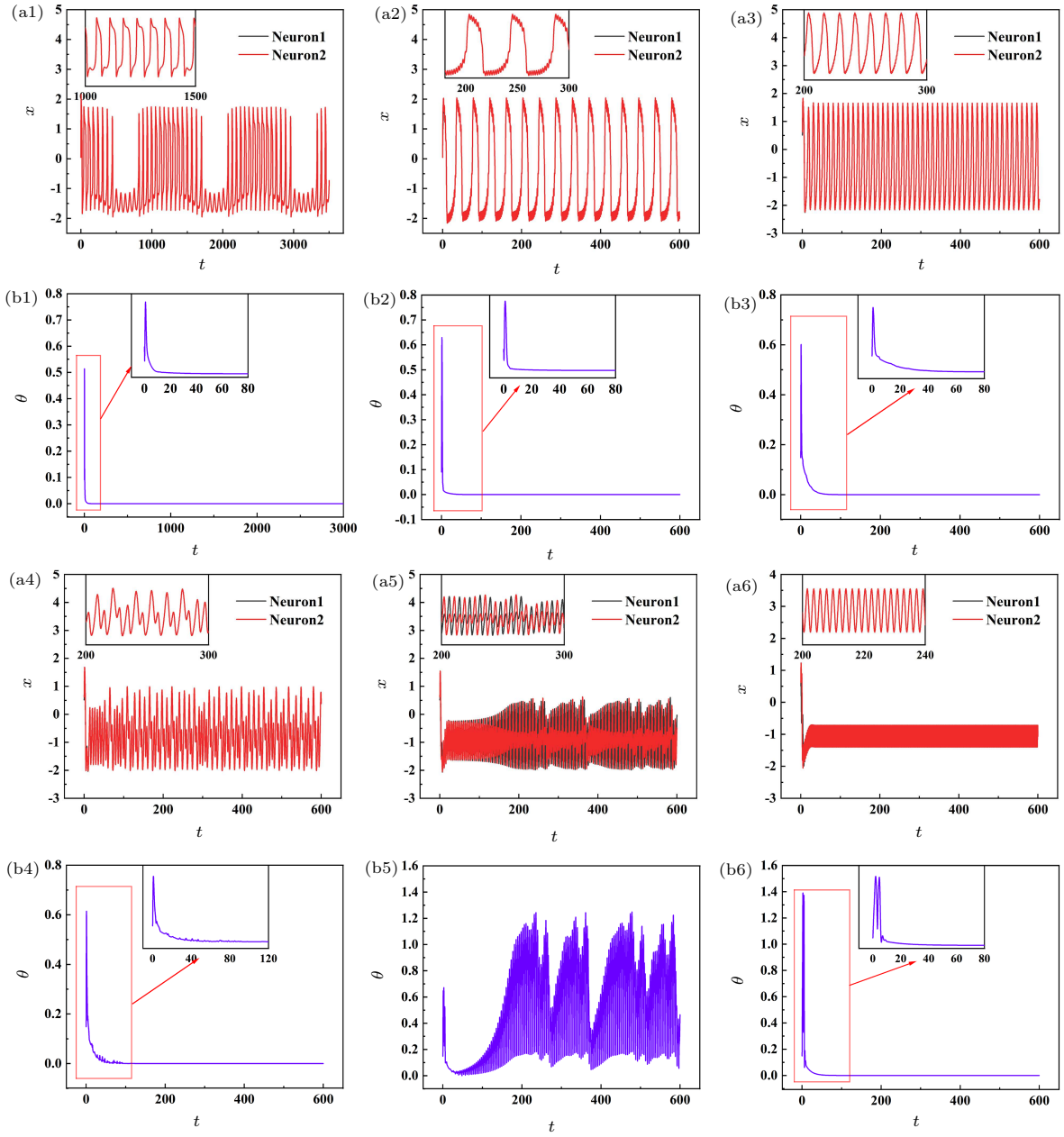


Fig. 4. Evolution diagrams of membrane potentials x_i ($i = 1, 2$) and the corresponding error function θ with sampling time under different angular frequencies ω when $N = 20$. Some parameter values are $A = 1.0$ and $\gamma = 0.1$; others are given in the text: (a1), (b1) $\omega = 0.005$; (a2), (b2) $\omega = 0.15$; (a3), (b3) $\omega = 0.5$; (a4), (b4) $\omega = 1.0$; (a5), (b5) $\omega = 1.5$; (a6), (b6) $\omega = 3.0$.

For $\omega = 0.005$, the evolution of membrane potential x_i and the corresponding error function θ with sampling time under different signal frequency ratios N, such as $N = 5$, 20, 25, is shown in Fig. 5. From Figs. 5(b1)–(b3) it can be seen that for three different signal frequency ratios N, the value of θ immediately reaches its maximum value and then rapidly drops to 0. This indicates that two coupled auditory neurons can quickly achieve synchronization, which is consistent with the result in Fig. 3. From Figs. 5(a1)–5(a3) it can be seen that with increasing N, two neurons maintain their cluster firing modes unchanged, despite some local differences. Therefore, the signal frequency ratio N has little effect on the firing mode of two coupled auditory neurons when $\omega = 0.005$.

As mentioned above, the dynamic behaviors of two coupled auditory neurons are synchronous when $\omega \in (0.0, 1.06) \cup (1.06, 1.35] \cup [2.42, 3.0]$ and $N \in [5, 35]$. When they are in a synchronous state, their firing modes are affected by the angular frequency ω for a constant signal frequency ratio N, while they are not affected by the signal frequency ratio N for a constant angular frequency ω.

3.2. Effects of signal angular frequency and coupling strength

Figure 4(a) shows that when $\omega = 0.005$, $A = 1.0$, $N = 20$ and $\gamma = 0.1$, the behaviors of the two coupled auditory neurons are synchronous. Therefore, in the following discussion the values of any two of the four parameters are kept unchanged, and the values of the other two parameters are changed to study their impact on the synchronization state.

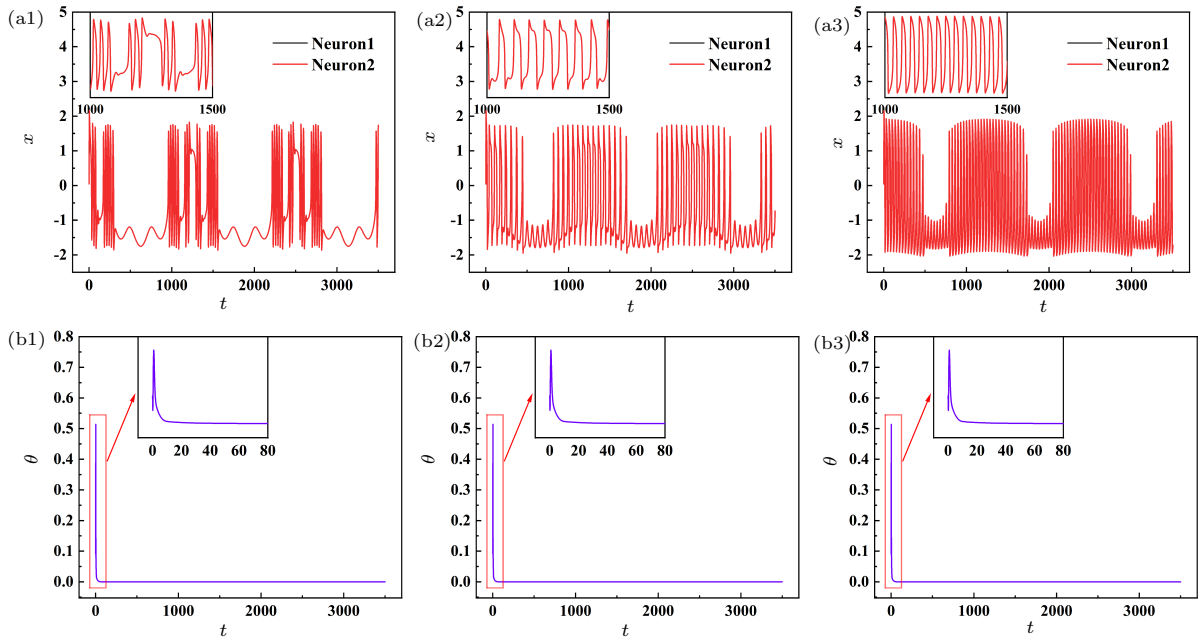


Fig. 5. Evolution diagrams of membrane potentials x_i ($i = 1, 2$) and corresponding error function θ with sampling time under different signal frequency ratios N when $\omega = 0.005$. Some parameter values are $A = 1.0$ and $\gamma = 0.1$, and others are given in the text: (a1), (b1) $N = 5$; (a2), (b2) $N = 20$; (a3), (b3) $N = 35$.

In this section, $A = 1.0$ and $N = 20$ are chosen for discussion. Correspondingly, the contour map of error function (θ) with angular frequency (ω) and coupling strength (γ) is shown in Fig. 6. From Section 2 it can be seen that $\gamma = 2e\rho CV_0/\hbar$. Here, e is the electron charge, i.e., $e = 1.6 \times 10^{-19}$, and $\hbar$ is the reduced Planck constant, i.e., $\hbar = 1.055 \times 10^{-34}$. Three parameters, ρ, C and V_0, are determined by the FHN circuit (ρ is the normalized resistance, V_0 is the cut-off voltage flowing through the nonlinear resistor and C is the capacitance). In the actual circuit, as long as the value of ρ is appropriate, γ can be guaranteed to be within the effective range.

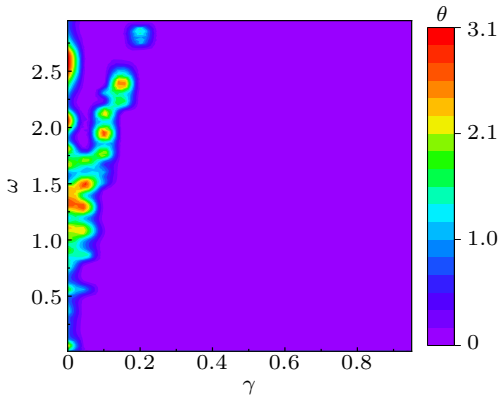


Fig. 6. The contour map of the error function (θ) with angular frequency (ω) and coupling strength (γ) when $A = 1.0$ and $N = 20$. Other parameter values and initial values are given in the text.

As can be seen from Fig. 6, in the region composed of coordinate points (0, 0), (0, 3.0) and (0.25, 3.0), most values of the error function θ are greater than 0. In this region, when $1.8 < \omega \leq 3.0$, the error function θ is 0 for some appropriate values of γ. Within the remaining range, the value of the error function $\theta = 0$. In addition, for different coupling strengths γ, the range of angular frequency ω that satisfies $\theta \neq 0$ varies. Therefore, for simplicity, some coupling strengths satisfying $0.25 \leq \gamma \leq 1.0$ should be considered to ensure that the behaviors of two coupled auditory neurons are synchronous.

Based on Fig. 6, for $\gamma = 0.5$, the evolution of membrane potential x_i and the corresponding error function θ with sampling time under different angular frequencies ω, such as $\omega = 0.005$, 0.15, 0.5, 1.0, 1.5, 3.0, is shown in Fig. 7. From Figs. 7(b1)–7(b6) it can be seen that when the angular frequency takes different values, the values of error function θ fluctuate slightly at the beginning and then quickly become 0 with increasing t. So, the behaviors of two coupled auditory neurons will soon reach synchronization. This finding is consistent with the results shown in Fig. 6. From Figs. 7(a1)–7(a6) it can be seen that for different angular frequencies ω, the firing modes of two neurons are different: the bursting firing state when $\omega = 0.005$, the spiking firing state when $\omega = 0.15$, the periodical firing state when $\omega = 0.5$, the chaotic firing state when $\omega = 1.0$ and the periodical firing state when $\omega = 1.5$ and $\omega = 3.0$. So, the angular frequency ω has an impact on the firing modes of the two coupled auditory neurons when $\gamma = 0.5$.

Figure 4 also shows the evolution of membrane potential x_i and the corresponding error function θ with sampling time under different angular frequencies ω when $\gamma = 0.1$. In this case, the behaviors of two coupled auditory neurons are asynchronous when $\omega = 1.5$, while for the other ω they are synchronous, which is consistent with the results shown in Fig. 6. In addition, the angular frequency ω has an impact on the firing modes of the two coupled auditory neurons.

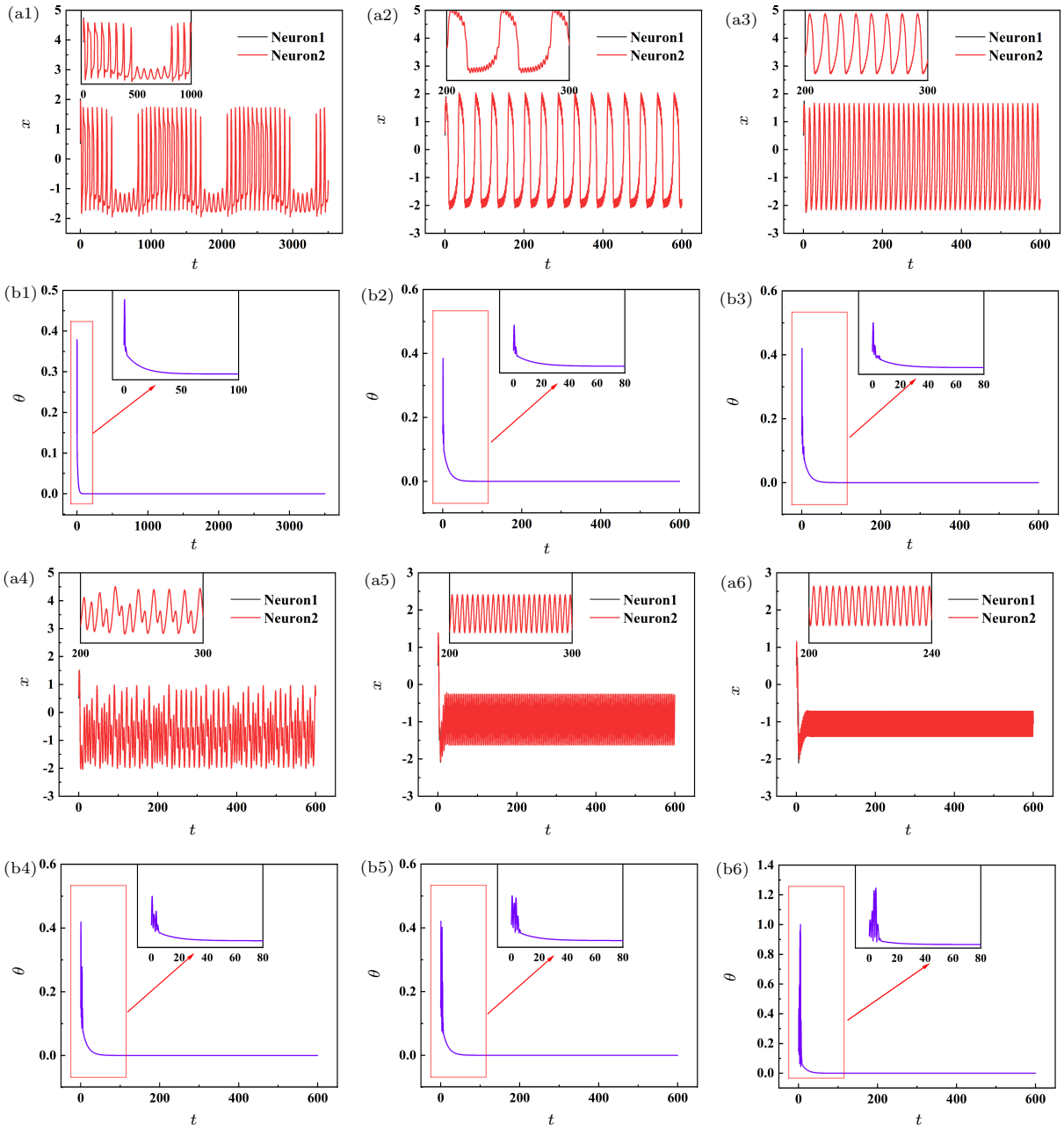


Fig. 7. Evolution diagrams of membrane potentials x_i ($i = 1, 2$) and the corresponding error function θ with sampling time under different angular frequencies ω when $\gamma = 0.5$. Some parameter values are $A = 1.0$ and $N = 20$, and others are given in the text: (a1), (b1) $\omega = 0.005$; (a2), (b2) $\omega = 0.15$; (a3), (b3) $\omega = 0.5$; (a4), (b4) $\omega = 1.0$; (a5), (b5) $\omega = 1.5$; (a6), (b6) $\omega = 3.0$.

On the other hand, for $\omega = 1.5$, the evolution of membrane potential x_i and the corresponding error function θ with sampling time under different coupling strengths γ, such as $\gamma = 0.3$, 0.5, 0.8, are shown in Fig. 8. From Figs. 8(b1)–8(b3) it can be seen that the value of θ fluctuates at the beginning, and then quickly becomes 0 with increasing t. So, the neurons can become synchronous quickly. This finding is consistent with the results shown in Fig. 6. From Figs. 8(a1)–8(a3) it can be seen that both neurons exhibit periodical firing states for three different coupling strengths γ. Therefore, when $\omega = 1.5$, $0.3 \leq \gamma \leq 1.0$, the behaviors of two coupled auditory neurons are synchronous, and the coupling strength γ has no impact on their firing modes.

As mentioned above, when $0.25 \leq \gamma \leq 1.0$ and $0.0 < \omega \leq 3.0$, the behaviors of two coupled auditory neurons are synchronous. When they are in a synchronous state, their firing modes are affected by the angular frequency ω for a constant coupling strength γ, while they are not affected by the coupling strength γ for a constant angular frequency ω.

3.3. Effects of signal angular frequency and low-frequency signal amplitude

In this section, $\gamma = 0.1$ and $N = 20$ are chosen for discussion. Correspondingly, the contour map of error function (θ) with angular frequency (ω) and coupling strength (γ) is shown in Fig. 9. It can be seen that in the triangular region of

$\omega \in [1.5, 2.3]$ and $A \in [0.65, 1.0]$, the value of the error function $\theta > 0$, and the behaviors of two coupled auditory neurons are asynchronous. In the remaining region, for simplicity, $\omega \in (0.0, 1.5) \cup (2.3, 3.0]$, $A \in (0.0, 1.0]$ and $\omega \in [1.5, 2.3]$, $A \in (0.0, 0.65)$, the value of error function $\theta = 0$ and the behaviors of two coupled auditory neurons are synchronous.

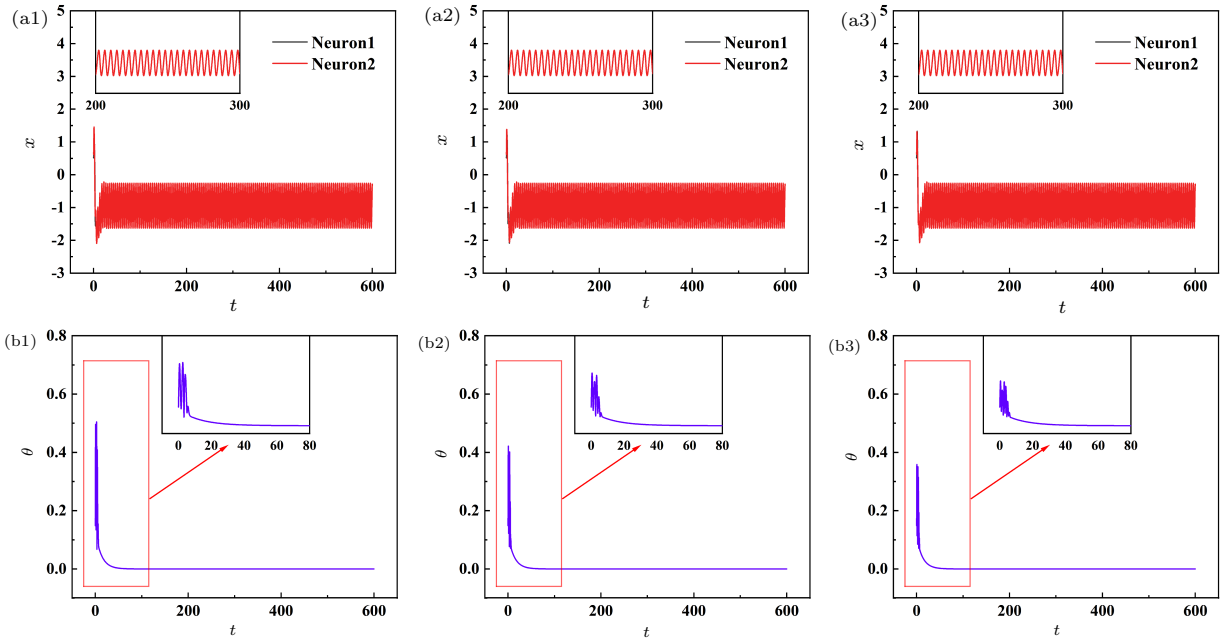


Fig. 8. Evolution diagrams of membrane potentials x_i ($i = 1, 2$) and the corresponding error function θ with sampling time under different coupling strengths γ when $\omega = 1.5$. Some parameter values are $A = 1.0$ and $N = 20$, and others are given in the text: (a1), (b1) $\gamma = 0.3$; (a2), (b2) $\gamma = 0.5$; (a3), (b3) $\gamma = 0.8$.

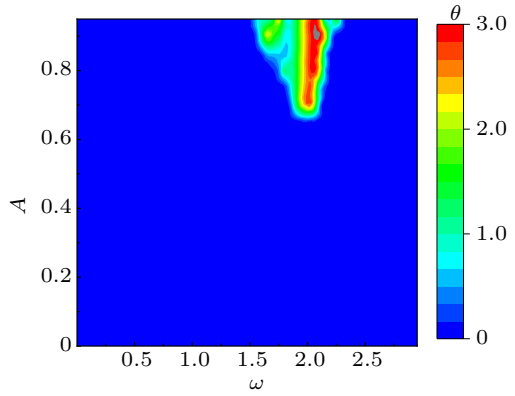


Fig. 9. Contour map of the error function (θ) with angular frequency (ω) and low-frequency signal amplitude (A) when $N = 20$ and $\gamma = 0.1$. Other parameter values and initial values are given in the text.

Based on Fig. 9, for $\omega = 0.005$, the evolution of membrane potential x_i and the corresponding error function θ with sampling time under different low-frequency signal amplitudes A, such as $A = 0.2$, 0.6, 1.0, is shown in Fig. 10. From Figs. 10(b1)–10(b3) it can be seen that when A takes different values, the evolution curves of the error function θ over sampling time are almost identical. The value of θ reaches its maximum value immediately after $t = 0$, and then rapidly drops to 0. This indicates that for different low-frequency signal amplitudes A, two coupled auditory neurons will quickly reach synchronization when $\omega = 0.005$, which is consistent with the result in Fig. 9. From Figs. 10(a1)–10(a3) it can be seen that as A increases, the dynamic behaviors of the two coupled auditory neurons change from a spiking firing state to a bursting firing state. Therefore, the low-frequency signal amplitude A has an impact on the firing mode of two coupled auditory neurons when $\omega = 0.005$.

Furthermore, for $\omega = 2.0$, the evolution of membrane potential x_i and the corresponding error function θ with sampling time under different low-frequency signal amplitudes A is shown in Fig. 11. From Figs. 11(b1)–11(b3) it can be seen that when $A = 0.2$ or 0.6 the behaviors of two coupled auditory neurons are synchronous, and when $A = 1.0$ they are asynchronous, which is consistent with the result in Fig. 9. As can be seen from Figs. 11(a1)–11(a3), with increasing of A, the amplitude of the membrane potential of two coupled auditory neurons will gradually increase, while their firing state remains unchanged. Therefore, when $\omega = 2.0$, the behaviors of two coupled auditory neurons will be synchronous only when A has an appropriate value. In addition, the value of A affects the amplitude of the membrane potential.

On the other hand, Fig. 4 also shows the evolution of membrane potential x_i and the corresponding error function θ with sampling time under different angular frequencies ω when $A = 1.0$. In this case, the behaviors of two coupled auditory neurons are asynchronous when $\omega = 1.5$, while for the other values of ω they are synchronous, which is consistent with the results shown in Fig. 9. In addition, the angular frequency ω has an impact on the firing modes of the two coupled auditory neurons.

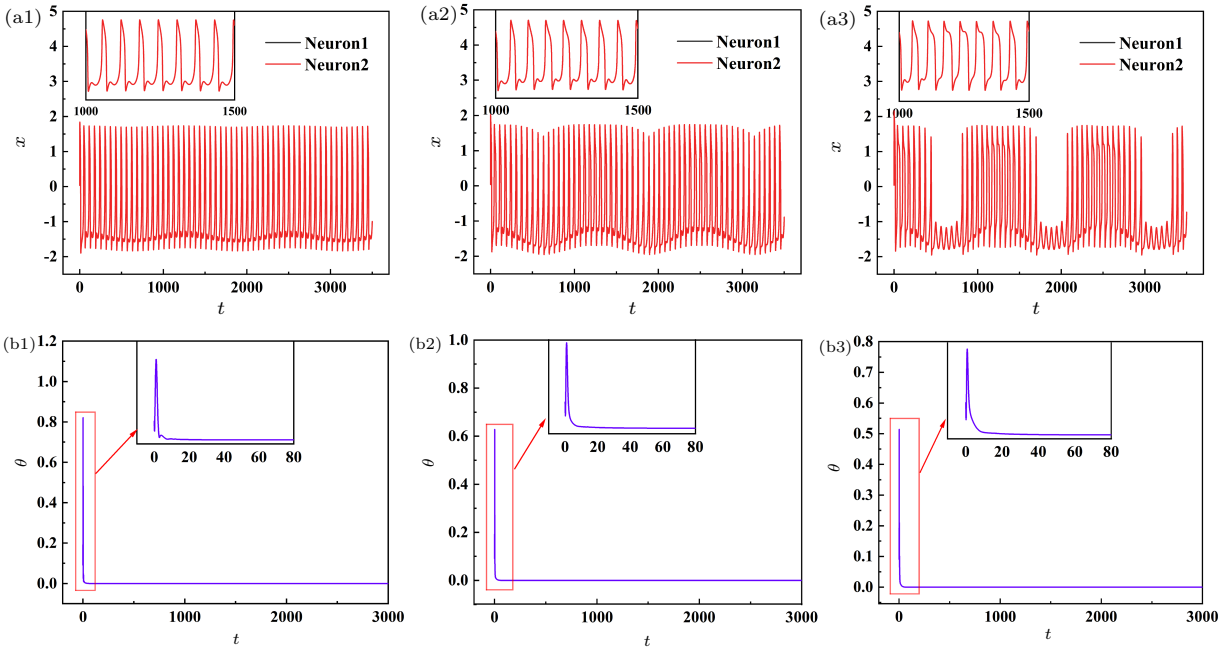


Fig. 10. Evolution diagrams of membrane potentials x_i ($i = 1, 2$) and the corresponding error function θ with sampling time under different low-frequency signal amplitudes A when $\omega = 0.005$. Some parameter values are $N = 20$ and $\gamma = 0.1$, and others are given in the text: (a1), (b1) $A = 0.2$; (a2), (b2) $A = 0.6$; (a3), (b3) $A = 1.0$.

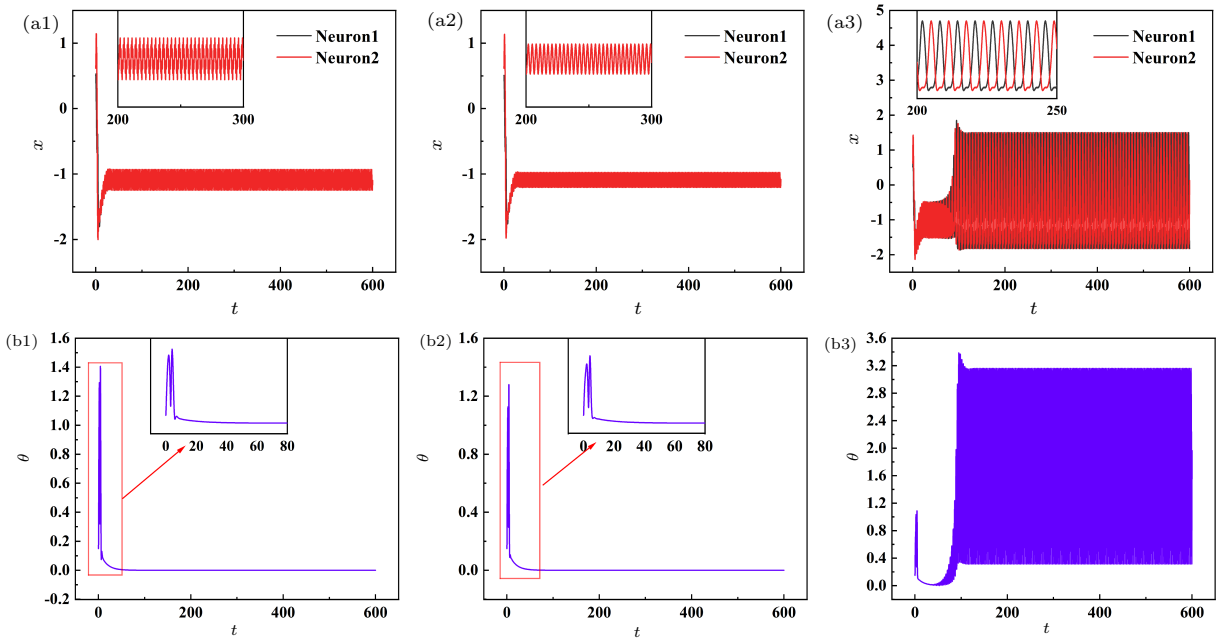


Fig. 11. Evolution diagrams of membrane potentials x_i ($i = 1, 2$) and the corresponding error function θ with sampling time under different low-frequency signal amplitudes A when $\omega = 2.0$. Some parameter values are $N = 20$ and $\gamma = 0.1$, and others are given in the text: (a1), (b1) $A = 0.2$; (a2), (b2) $A = 0.6$; (a3), (b3) $A = 1.0$.

As mentioned above, as $\omega \in (0.0, 1.5) \cup (2.3, 3.0]$, $A \in (0.0, 1.0]$ and $\omega \in [1.5, 2.3]$, $A \in (0.0, 0.65)$, the behaviors of two coupled auditory neurons are synchronous. When they are in a synchronous state, their firing modes are affected by the angular frequency ω and the low-frequency signal amplitude A. In addition, the value of A can affect the amplitude of the membrane potential.

3.4. Effects of signal frequency ratio and low-frequency signal amplitude

Firstly, $\gamma = 0.1$ and $\omega = 0.005$ are selected for discussion in this section. Correspondingly, the contour map of the error function (θ) with signal frequency ratio (N) and low-frequency signal amplitude (A) is shown in Fig. 12. It is found that for any N and A in the range $0.0 < A \leq 1.0$ and $5 \leq N \leq 35$, the value of error function $\theta = 0$, which indicates that the dynamic behaviors of two coupled auditory neurons are always synchronous.

Based on Fig. 12, considering $A = 0.2$, the evolution of membrane potential x_i and the corresponding error function θ with sampling time under different signal frequency ratios N, such as $N = 5$, 20, 35, is shown in Fig. 13. From Figs. 13(b1)–13(b3) it can be seen that when N takes different values, the evolution curves of error function θ over sampling time are almost identical from overall to local. The value of θ reaches its maximum value immediately after $t = 0$, rapidly drops to 0, fluctuates slightly and finally quickly reaches 0. This indicates that the two coupled auditory neurons will quickly achieve synchronization, which is consistent with the result in Fig. 12. From Figs. 13(a1)–13(a3) it can be seen that when the value of N is different, neurons exhibit various firing states: bursting firing when $N = 5$, spiking firing when $N = 20$ and periodical firing when $N = 35$. Therefore, the signal frequency ratio N has an impact on the firing mode of two coupled auditory neurons when $A = 0.2$.

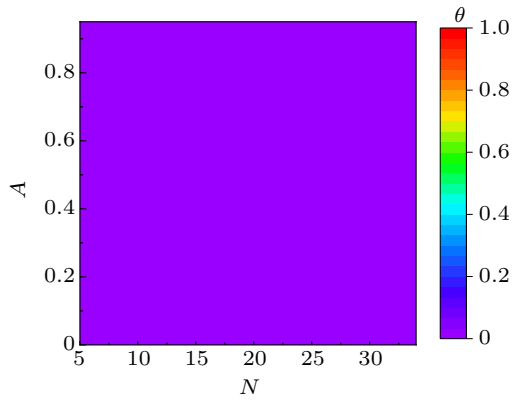


Fig. 12. Contour map of the error function (θ) with signal frequency ratio (N) and low-frequency signal amplitude (A) when $\omega = 0.005$ and $\gamma = 0.1$. Other parameter values and initial values are given in the text.

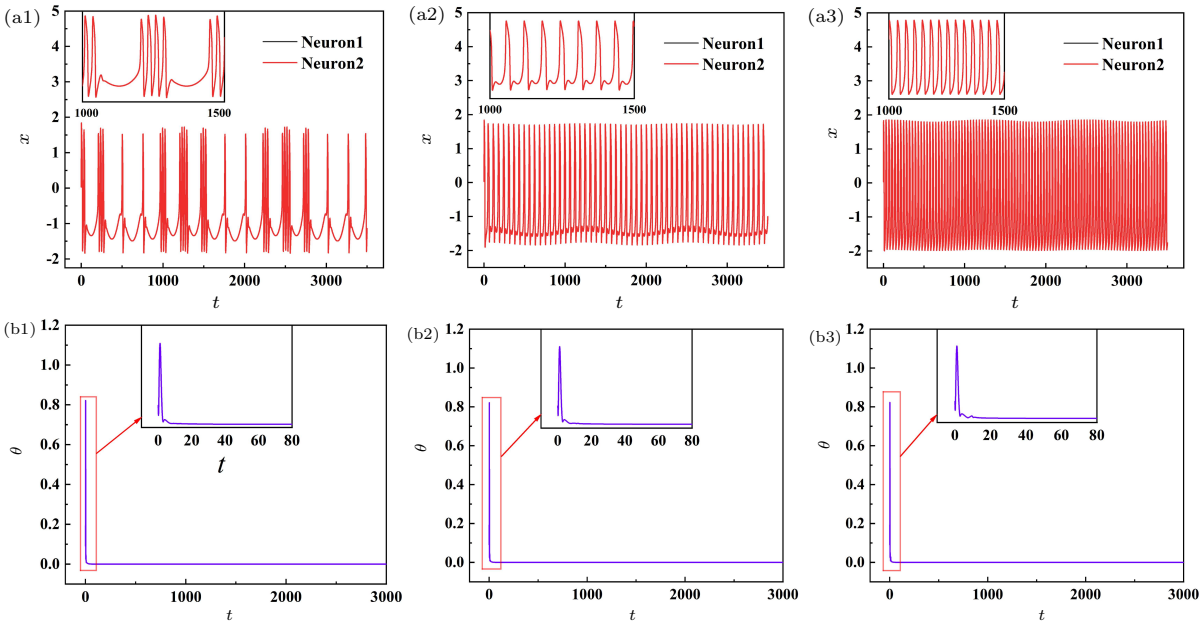


Fig. 13. Evolution diagrams of membrane potential x_i ($i = 1$, 2) and the corresponding error function θ with sampling time under different signal frequency ratios N when $A = 0.2$. Some parameter values are $\omega = 0.005$ and $\gamma = 0.1$, and others are given in the text: (a1), (b1) $N = 5$; (a2), (b2) $N = 20$; (a3), (b3) $N = 35$.

On the other hand, Fig. 10 also shows the evolution of membrane potential x_i and the corresponding error function θ with sampling time under different low-frequency signal amplitudes A as $N = 20$. In this case, for three different low-frequency signal amplitudes A, two coupled auditory neurons will quickly reach synchronization, which is consistent with the result in Fig. 11. In addition, the low-frequency signal amplitude A has an impact on the firing mode of two coupled auditory neurons.

Secondly, $\gamma = 0.1$ and $\omega = 2.0$ are selected for discussion, because as can be seen from Figs. 3, 6 and 9, when $\omega = 2.0$, the synchronization characteristics of two auditory neurons will change. The frequency of the HLF sound signal increases and its period decreases. Too short a time is not enough to synchronize the dynamic behaviors of two auditory neurons. Correspondingly, the contour map of error function (θ) and signal frequency ratio (N) and low-frequency signal amplitude (A) is shown in Fig. 14. From Figs. 14(b1)–14(b3) it is found that when $0.0 < A \leq 0.65$ and $5 \leq N \leq 35$ the value of error function $\theta = 0$ and when $0.65 < A \leq 1.0$ and $5 \leq N \leq 35$ the value of error function $\theta > 0$.

Based on Fig. 14, considering $A = 0.6$, the evolution of membrane potential x_i and the corresponding error function θ with sampling time under different signal frequency ratios N is shown in Fig. 15. From Figs. 15(b1)–15(b3) it can be seen that when N takes different values, the two coupled auditory neurons will quickly achieve synchronization, which is consistent with the result in Fig. 14. From Figs. 15(a1)–15(a3) it can be seen that when the value of N is different, neurons remain in the same firing state.

On the other hand, Fig. 11 also shows the evolution of membrane potential x_i and the corresponding error function θ with sampling time under different low-frequency signal amplitudes A as $N = 20$. In this case, with increasing A the dynamic behaviors of two coupled auditory neurons change from synchronous to asynchronous, which is consistent with the result in Fig. 14. In addition, the low-frequency signal amplitude A has an impact on the amplitude of the membrane potential.

As mentioned above, when $\omega = 0.005$, the dynamic behaviors of two auditory neurons are always synchronous as $0.0 < A \leq 1.0$ and $5 \leq N \leq 35$, and their firing modes are influenced by the frequency ratio N and the low-frequency signal amplitude A. When $\omega = 2.0$, the dynamic behaviors of two auditory neurons are synchronous as $0.0 < A \leq 0.65$ and $5 \leq N \leq 35$. When they are in a synchronous state, their firing modes are not influenced by the frequency ratio N and the low-frequency signal amplitude A. But the value of A affects the amplitude of membrane potential.

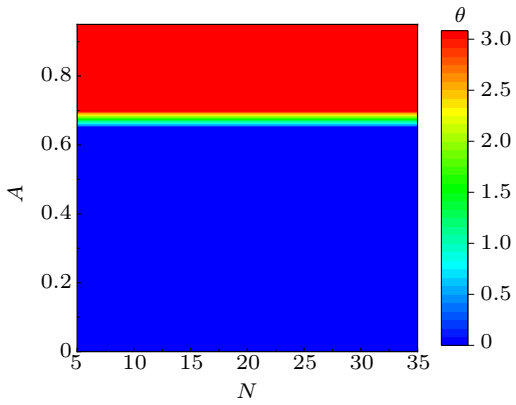


Fig. 14. Contour map of the error function (θ) with signal frequency ratio (N) and low-frequency signal amplitude (A) when $\omega = 2.0$ and $\gamma = 0.1$. Other parameter values and initial values are given in the text.

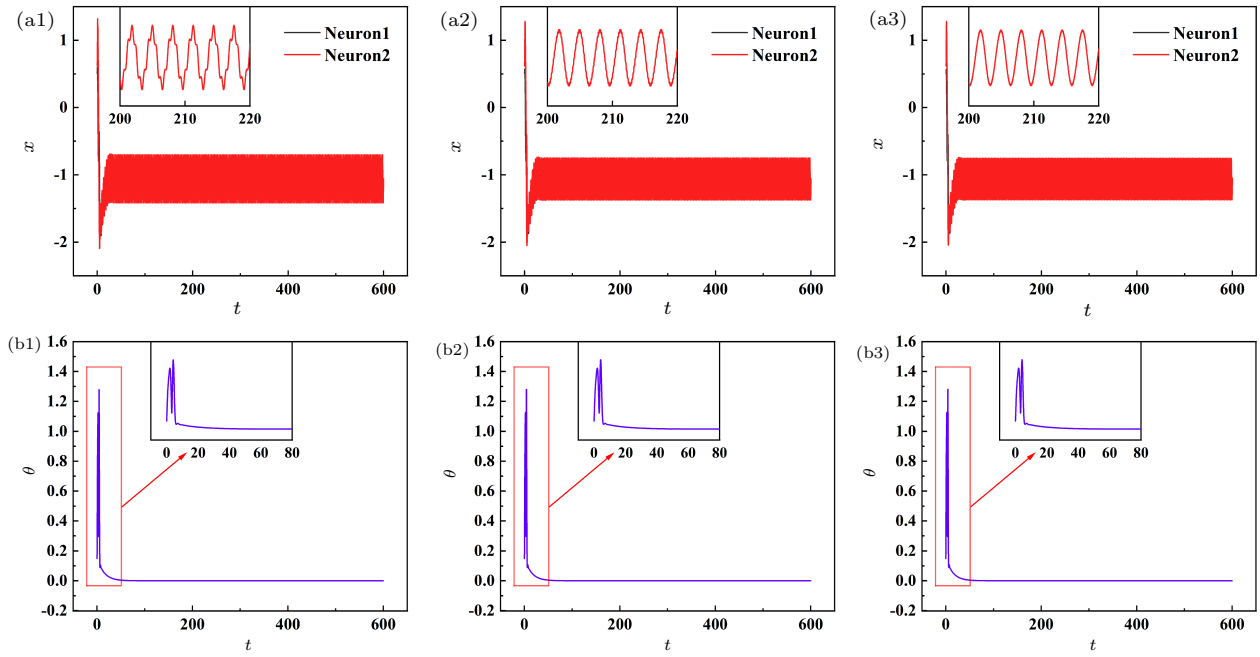


Fig. 15. Evolution diagrams of membrane potential x_i ($i = 1, 2$) and the corresponding error function θ with sampling time under different signal frequency ratios N when $A = 0.6$. Some parameter values are $\omega = 2.0$ and $\gamma = 0.1$, and others are given in the text: (a1), (b1) $N = 5$; (a2), (b2) $N = 20$; (a3), (b3) $N = 35$.

3.5. Effects of signal frequency ratio and coupling strength

In this section, $A = 1.0$ and $\omega = 0.005$ are chosen for discussion. Correspondingly, the contour map of error function (θ) with signal frequency ratio (N) and coupling strength (γ) is shown in Fig. 16. It can be seen that for any valid N, $\theta > 0$ at $0.0 < \gamma < 0.05$ and $\theta = 0$ at $0.05 \leq \gamma \leq 1.0$. Therefore, as long as the coupling strength $\gamma \geq 0$, the dynamic behaviors of two coupled auditory neurons are synchronous.

Based on Fig. 16, considering $N = 20$, the evolution of membrane potential x_i and the corresponding error function θ with sampling time under different coupling strengths γ, such as $\gamma = 0.0$, 0.01, 0.05, 0.1, 0.2, is shown in Fig. 17. From Fig. 17(b1) it can be seen that $\theta > 0$ at $\gamma = 0.0$. So the behaviors of two coupled auditory neurons are entirely asynchronous. When the coupling strength slightly increases, such as $\gamma = 0.01$, although the value of θ oscillates somewhat at the beginning it quickly becomes zero, as seen in Fig. 17(b2). As the coupling strength continues to increase, such as $\gamma = 0.05$, 0.1, 0.2, as shown in Figs. 17(b3)–17(b5), respectively, the value of θ is not zero at first but quickly becomes zero. Therefore, the behaviors of two coupled auditory neurons can quickly reach synchronization. From Figs. 17(a1)–17(a5) it can be seen that with increasing γ, the firing modes of two coupled auditory neurons do not change. Therefore, when signal frequency ratio N is constant, the coupling strength γ has no impact on the firing mode of two coupled auditory neurons.

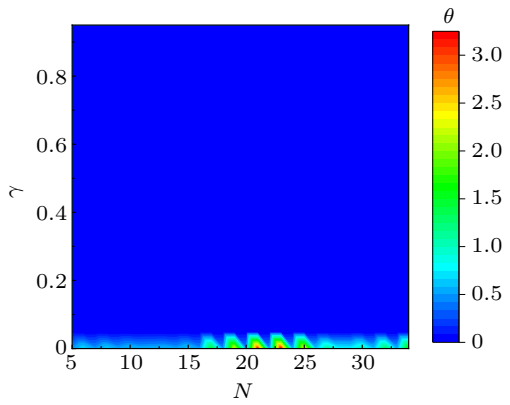


Fig. 16. Contour map of the error function (θ) with signal frequency ratio (N) and coupling strength (γ) when $A = 1.0$ and $\omega = 0.005$. Other parameter values and initial values are given in the text.

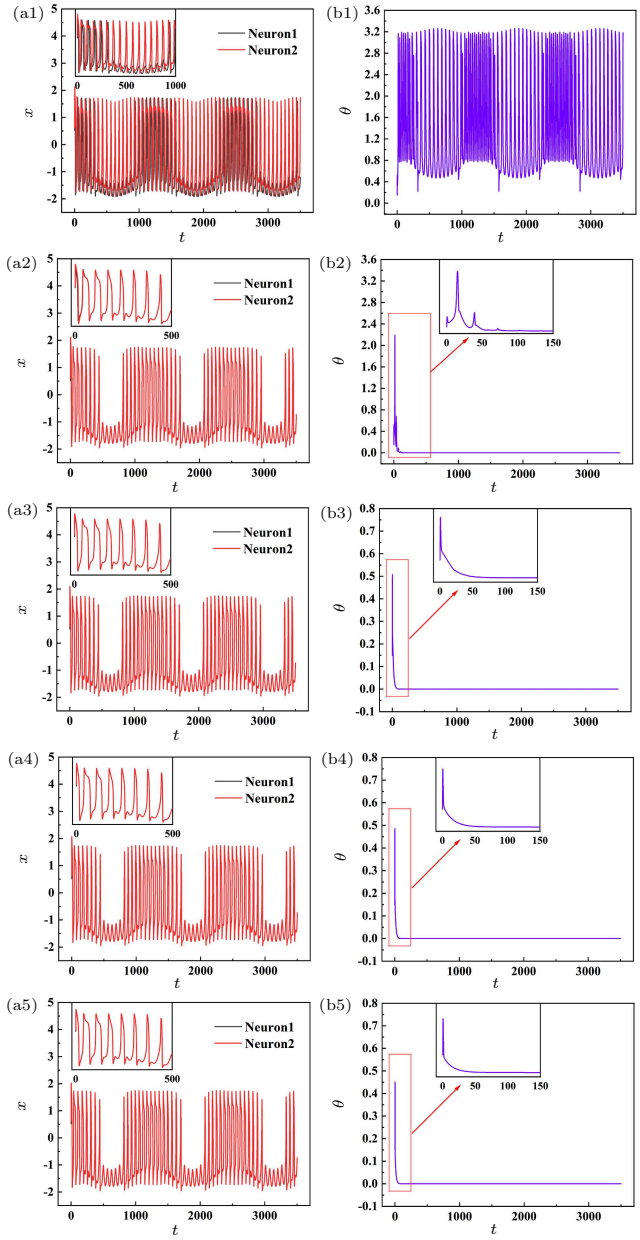


Fig. 17. Evolution diagrams of membrane potential x_i ($i = 1, 2$) and corresponding error function θ with sampling time under different coupling strengths γ when $N = 20$. Some parameter values are $A = 1.0$ and $\omega = 0.005$, and others are given in the text: (a1), (b1) $\gamma = 0.0$; (a2), (b2) $\gamma = 0.01$; (a3), (b3) $\gamma = 0.05$; (a4), (b4) $\gamma = 0.1$; (a5), (b5) $\gamma = 0.2$.

On the other hand, Fig. 5 also shows the evolution of membrane potential x_i and corresponding error function θ with sampling time under different signal frequency ratios N when $\gamma = 0.1$. In this case, the dynamical behaviors of the two coupled auditory neurons are synchronous for three different signal frequency ratios, and the signal frequency ratio N has no impact on their firing mode.

As mentioned above, as long as the coupling channel exists, the dynamic behavior of the two coupled auditory neurons is always synchronous. Moreover, their firing modes are not affected by the coupling strength γ or the signal frequency ratio N.

3.6. Effects of low-frequency signal amplitude and coupling strength

In this section, $N = 20$ and $\omega = 0.005$ are chosen for discussion. Correspondingly, the contour map of error function (θ) with coupling strength (γ) and low-frequency signal amplitude (A) is shown in Fig. 18. It is found that for any γ and A in the range of $0.0 < \gamma \leq 1.0$ and $0.0 < A \leq 1.0$, the value of error function $\theta = 0$, which indicates that the dynamic behaviors of two coupled auditory neurons are always synchronous.

Figure 10 also shows the evolution of membrane potential x_i ($i = 1, 2$) and the corresponding error function θ with sampling time under different low-frequency signal amplitudes A when $\gamma = 0.1$. In this case, for three different low-frequency signal amplitudes A, two coupled auditory neurons will quickly reach synchronization, which is consistent with the result in Fig. 18. Also, the low-frequency signal amplitude A has an impact on their firing modes.

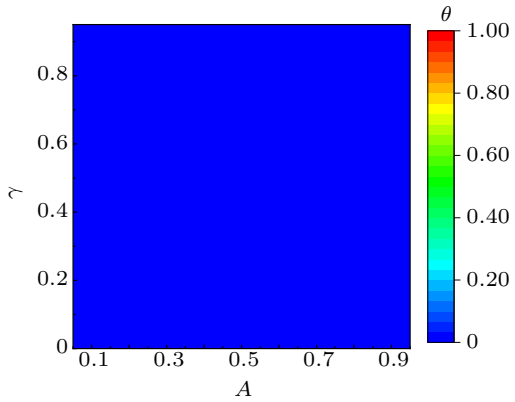


Fig. 18. The contour map of the error function (θ) with coupling strength (γ) and low-frequency signal amplitude (A) when $\omega = 0.005$ and $N = 20$. Other parameter values and initial values are given in the text.

On the other hand, Fig. 17 also shows the evolution of membrane potential x_i and the corresponding error function θ with sampling time under different coupling strengths γ when $A = 1.0$. In this case, the dynamical behaviors of two coupled auditory neurons are always synchronous as long as the coupling channel exists, and their firing modes are not affected by the coupling strength γ.

As mentioned above, as long as the coupling channel exists, the dynamic behaviors of two coupled auditory neurons are always synchronous. In addition, their firing modes are not affected by the coupling strength γ but are affected by the low-frequency signal amplitude A.

4. Discussion and conclusion

Piezoelectric ceramic is an intelligent material that converts mechanical effects (such as pressure, motion or vibration) into electrical signals, and vice versa. In a FHN neuron circuit, if piezoelectric ceramic is used instead of a time-varying voltage source, external sound signals can be sensed and received, thereby constructing a mono-ear auditory neuron. To establish a binaural auditory neuron system, a parallel circuit consisting of a Josephson junction and a linear resistor is used to couple two auditory neurons. The Josephson junction can simulate the pulse signal transmission mode of the brain and also has a very low energy consumption. On the other hand, the linear resistor can carry some current to protect the Josephson junction. Since signals from accurate signal sources rarely present a single frequency, and neurons can receive multiple signal inputs synchronously through various channels, the HLF signal is used as external sound source to drive the binaural auditory system. Only frequency ratios greater than 5 are considered to highlight the presence of the high-frequency signal, i.e., $N \geq 5$.

According to Kirchhoff's law, the circuit equation of the binaural auditory system can be obtained, which can be transformed into a dimensionless equation through scaling transformation. Based on this dimensionless equation, the synchronization and mode transition of two coupled auditory neurons can be studied through simulation. As long as ω participates in regulation, whether related to N, γ or A, the dynamic behaviors of two coupled auditory neurons will exhibit asynchronous phenomena within a specific parameter range, as shown in Subsections 3.1–3.3; If any two of N, γ, and A are selected as adjustment parameters, that is, ω is chosen appropriately and remains unchanged, the dynamic behaviors of two coupled auditory neurons are always synchronous within the effective range of the parameters, as shown in Subsections 3.4–3.6.

Therefore, the angular frequency ω of the sound signal is a significant factor that affects the synchronization of dynamic behaviors of two coupled neurons in the human binaural auditory system. When their behaviors reach synchronization, their firing modes are influenced by the physical characteristics of the HLF signal, including angular frequency ω, low-frequency signal amplitude A and signal frequency ratio N, without being affected by coupling strength γ. Correspondingly, in real life, inappropriate pitch can lead to asynchronous dynamic behaviors of two coupled neurons. In addition, the pitch, intensity and signal frequency ratio can all cause changes in their firing modes. Asynchronous dynamic behavior and changes in firing modes can cause damage to the human binaural auditory neuron system, leading to hearing impairment.

A recent study has shown that two identical piezoelectric sensing neurons driven by the same periodic stimulus can achieve synchronization without synaptic coupling.[2] This result is different from the one we obtained because the external sound signals used are different. Reference [2] used a cosine sound signal, while a HLF signal was used in this paper. However, from our discussion it can be seen that if (ω, γ) or (N, γ) are selected as control parameters, when there is no coupling between two auditory neurons, namely $\gamma = 0$, their dynamic behaviors cannot achieve synchronization; however, if selecting (A, γ) as the adjustment parameters, their dynamic behaviors can achieve synchronization regardless of whether they are coupled or not.

In real life, external sound signals are not always regular. If the external sound signal is noise, what impact will it have on the dynamic behavior of the binaural system? In addition, the coupling patterns between two auditory neurons may be diverse, and what impact will different coupling patterns have on their dynamic behaviors? When two neural circuits are connected through a capacitor, some field energy is stored in the coupling channel and then sent back to the coupled neural circuit to achieve energy balance.[41] In this binaural system, how is the energy between two neurons balanced? These are issues worthy of further discussion, and some interesting results are expected to be achieved.

Acknowledgement

Project supported by the National Natural Science Foundation of China (Grant No. 11605014).

References

[1] Rubel E W and Fritzsch B 2002 *Annu. Rev. Neurosci.* **25** 51
[2] Zhou P, Yao Z, Ma J and Zhu Z G 2021 *Chaos Soliton. Fract.* **145** 110751
[3] Guo Y, Zhou P, Yao Z and Ma J 2021 *Nonlinear Dyn.* **105** 3603
[4] Ma J 2022 *Journal of Guangxi Normal University* (Natural Science Edition) **40** 307
[5] Lu L L, Jia Y, Xu Y, Ge M Y, Yang L J and Zhan X 2019 *Sci. China Technol. Sci.* **62** 427
[6] Lu L L, Jia Y, Liu W H and Yang L J 2017 *Complexity* **2017** 7628537
[7] Wang G W, Xu Y, Ge M Y, Jia Y and Lu L L 2020 *Int. J. Electron. Commun. (AEU)* **120** 153209
[8] Wang Y, Wang C N, Ren G D, Jin W Y and Tang J 2017 *Nonlinear Dyn.* **89** 1967
[9] Wang G W, Yu D, Ding Q M, Li T Y and Jia Y 2021 *Chaos Soliton. Fract.* **150** 111210
[10] Chua L 2014 *Semicond. Sci. Tech.* **29** 104001
[11] Hong Q H, Zhao L and Wang X P 2019 *Neurocomputing* **330** 11
[12] Juzekaeva E, Nasretdinov A, Battistoni S, Berzina T, Iannotta S, Khazipov R, Erokhin V and Mukhtarov M 2019 *Adv. Mater. Technol.* **4** 1800350
[13] Yang Z Q, Zhang Y and Wu F Q 2020 *Nonlinear Dyn.* **100** 647

[14] Wu F Q, Zhang Y and Zhang X J 2019 *Nonlinear Dyn.* **98** 971
[15] Jin W Y, Wang A, Ma J and Lin Q 2019 *Sci. China Technol. Sc.* **62** 2113
[16] Shan Y, Yang H, Wang H, Zhang S, Li Y and Xu G 2022 *Chin. Phys. B* **31** 080507
[17] Lukić J and Denić D 2015 *Metrol. Meas. Syst.* **22** 351
[18] Xu Y, Liu M, Zhu Z and Ma J 2020 *Chin. Phys. B* **29** 098704
[19] Li Z, Xie W, Zeng J and Zeng Y 2023 *Chin. Phys. B* **32** 010503
[20] Guo Z, Li Z, Wang M and Ma M 2023 *Chin. Phys. B* **32** 038701
[21] Zhang X F, Wang C N, Ma J and Ren G D 2020 *Mod. Phys. Lett. B* **34** 050267
[22] Xu Y, Guo Y Y, Ren G D and Ma J 2020 *Appl. Math. Comput.* **385** 125427
[23] Qi G and Wang Z 2021 *Chin. Phys. B* **30** 120516
[24] Nakayama T 1985 *Jpn. J. Physiol.* **35** 375
[25] Liu Y, Xu W J, Ma J, Alzahrani F and Hobiny A 2020 *Front. Inform. Technol. Electron. Eng.* **21** 1387
[26] Liu Y, Xu Y and Ma J 2020 *Commun. Nonlinear Sci. Numer. Simul.* **89** 105297
[27] Guo Y Y, Zhu Z G, Wang C N and Ren G D 2020 *Optik* **218** 164993
[28] Xie Y, Yao Z, Hu X and Ma J 2021 *Chin. Phys. B* **30** 120510
[29] Pountougnigni O V, Yamapi R, Filatrella G and Tchawoua C 2019 *Phys. Rev. E* **99** 032220
[30] Koudafoke G N, Hinvi L A, Miwadinou C H, Monwanou A V and Orou J C 2021 *Sens. Actuat. A: Phys.* **318** 112509
[31] Zhang Y, Zhou P, Tang J and Ma J 2021 *Chin. J. Phys.* **71** 72
[32] Zhang Y, Xu Y, Yao Z and Ma J 2020 *Nonlinear Dyn.* **102** 1849
[33] Zhang Y, Wang C N, Tang J, Ma J and Ren G D 2020 *Sci. China Technol. Sc.* **63** 2328
[34] Schneider M L, Donnelly C A and Russek S E 2018 *J. Appl. Phys.* **124** 161102
[35] Attwell D and Laughlin S B 2001 *J. Cerebr. Blood F. Met.* **21** 1133
[36] Hodgkin A L and Huxley A F 1952 *J. Physiol.* **117** 500
[37] FitzHugh R 1961 *Biophys. J.* **1** 445
[38] Nagumo J, Arimoto S and Yoshizawa S 1962 *Proceedings of the IRE* **50** 2061
[39] FitzHugh R 1968 *J. Appl. Physiol.* **25** 628
[40] Ge M Y, Jia Y, Xu Y and Yang L J 2018 *Nonlinear Dyn.* **91** 515
[41] Wang Y, Sun G and Ren G 2023 *Chin. Phys. B* **32** 040504